Phase Polymorphism of $[Mn(DMSO)_6](ClO_4)_2$ Studied by Differential Scanning Calorimetry

Anna Migdał-Mikuli and Elżbieta Szostak

Department of Chemical Physics, Faculty of Chemistry, Jagiellonian University, ulica Ingardena 3, 30-060 Kraków, Poland

Reprint requests to Dr. hab. A. M.-M.; Fax: +48-12-634-0515; E-mail: migdalmi@chemia.uj.edu.pl

Z. Naturforsch. **60a,** 289 – 295 (2005); received January 13, 2005

Six solid phases of $[Mn(DMSO)_6](ClO_4)_2$ have been detected by differential scanning calorimetry. The phase transitions were found between the following solid phases: stable KIc ↔ stable KIb at $T_{C5} = 225$ K, metastable KIII ↔ metastable KII at $T_{C4} = 322$ K, stable KIb → stable KIa at $T_{C3} = 365$ K, metastable KII ↔ overcooled K0 at $T_{C2} = 376$ K and stable KIa → stable K0 at $T_{C1} = 379$ K. The title compound melts at $T_m = 488$ K.

Key words: Hexadimethylsulphoxidemanganese(II) Chlorate(VII); Phase Transitions; Melting Point; DSC.

1. Introduction

Hexadimethylsulphoxidemanganese(II) chlorate (VII) (called HMnC) consists of two ions: $[Mn((CH_3)_2SO)_6]^{2+}$ and ClO_4^-. The cation is a slightly deformed octahedron, where the manganese atom is surrounded by six oxygen atoms coming from the dimethylsulphoxide (DMSO) ligands. The DMSO ligands are built like C_{2v} pyramids. So far the crystal structure of HMnC is unknown. However, the analogous compound $[Cd(DMSO)_6](ClO_4)_2$ crystallizes in the rhombic system (space group: No 43; $Fdd2$; C_{2v}^{19} [1]). We have recently investigated the polymorphism of $[Cd(DMSO)_6](ClO_4)_2$ (HCdC) and $[Co(DMSO)_6](ClO_4)_2$ (HCoC) by differential scanning calorimetry (DSC) [2, 3], and found that both substances have five solid phases. Three of them are stable and two are metastable phases. The high temperature phases of these compounds can be easily overcooled. The purpose of the present work was to carefully examine the polymorphism of HMnC in the temperature range of 173 – 530 K using DSC. Additionally, we compared the obtained results with those obtained earlier for HCdC [2] and HCoC [3].

2. Experimental

2.1. Sample Preparation

A few grams of $[Mn(H_2O)_6](ClO_4)_2$ were dissolved while being slowly heated up in DMSO of high chemical purity, which was previously additionally purified by vacuum distillation at low pressure and next was dehydrated by shaking with anhydrous CaH_2, according to requirements presented in [4]. This solution was then chilled and the precipitated crystals of HMnC were filtered and washed with acetone. They were then dried in a desiccator over phosphorous pentaoxide for a few hours. After desiccation, they were put in a sealed vessel and stored in a desiccator with barium oxide as a desiccant.

To check the chemical composition of the synthesised HMnC, the percentage content of manganese ions was checked using a complexometric method, with a solution of the sodium salt of ethylenediaminetetraacetic acid (EDTA) as a titrant. The theoretical content of manganese equalled 7.60%, and its content found by the titration analysis amounted to 7.51 ± 0.18%. The content of carbon and hydrogen in the DMSO ligand was determined using elementary analysis on an EURO EA 3000 apparatus. For carbon atoms, the difference between the theoretical value (19.95%) and the test value (19.31 ± 0.01%) did not exceed 0.1%. For hydrogen atoms, the theoretical value was 5.02% and the test value was 5.16 ± 0.01%. Therefore, the elementary analysis of the title compound confirmed the presence of the stoichiometric number of six DMSO molecules in the complex cation.

2.2. Sample Identification and Characteristics

In order to further identify the title compound, its infrared absorption spectra (FT-FIR and FT-MIR) and

0932–0784 / 05 / 0400–0289 $ 06.00

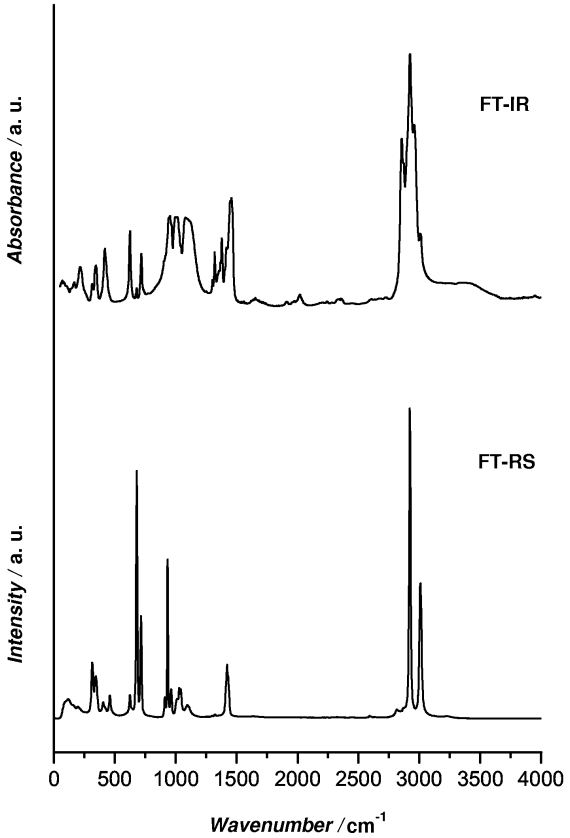

Fig. 1. Comparison of the infrared (FT-FIR and FT-MIR) and Raman (FT-RS) spectra of $[Mn(DMSO)_6](ClO_4)_2$.

its Raman spectrum (FT-RS) were recorded at ambient temperature. The FT-FIR and FT-MIR spectra were obtained using Digilab FTS-14 and EQUINOX-55 Bruker Fourier transform infrared spectrometers, respectively, with a resolution of 2 cm^{-1}. For powder samples, suspended in apiezon grease, the FT-FIR spectrum was recorded using polyethylene and silicon windows. The FT-MIR spectrum was recorded for a sample suspended in Nujol between the KBr pellets. The FT-RS spectrum was recorded using a Bio-Rad spectrometer with a YAG neodymium laser ($\lambda = 1064$ nm) at $10-4000$ cm^{-1} at a resolution of 4 cm^{-1}. Figure 1 presents a comparison of the infrared and Raman spectra of HMnC. Table 1 contains a list of the obtained and literature data [2–8] of band frequencies and their assignments. The recorded spectra additionally identify the investigated compound as $[Mn(DMSO)_6](ClO_4)_2$.

Thermal analysis of the examined compound was made in order to enable further verification of its composition. The thermogravimetric (TG) measurements and simultaneous differential thermal analysis (DTA) were performed using a Mettler Toledo TGA/SDTA 851^e apparatus. A sample weighing 10.9628 mg was placed in a 150 μl Pt/Rh crucible. The TG measurements were made in a flow of argon (80 ml/min) from 303 K up to 393 K at a constant heating rate of 2 K min^{-1}. The simultaneous evolved gas analysis (SEGA), with an on-line quadrupole mass spectrometer (QMS) using a Balzer GSD 300T apparatus, was

Table 1. The list of band positions of the Raman (FT-RS) and infrared spectra (FT-FIR and FT-MIR) of solid $[Mn(DMSO)_6](ClO_4)_2$ and liquid DMSO at room temperature (vw, very weak; w, weak; sh, shoulder; m, medium; st, strong; vst, very strong; br, broad).

Frequencies in cm^{-1}					
$[Mn(DMSO)_6](ClO_4)_2$			DMSO		
RS	IR		RS	IR	Assignments
this work	this work in KBr pellet	this work [a] in Apiezon [b] in Nujol	[4, 5]		
		68 w[a]			ν_L (lattice)
		77 w[a]			ν_L (lattice)
116 m		103 sh[a]			ν_L (lattice)
		134 w[a]			ν_L (lattice)
		168 m[a]			ν_d(MnO)
197 vw		216 st[a]			ν_d(MnO)
314 m		316 m[a]	313 m	313 w	δ_{as}(CSC)
343 m		344 st[a]	338 m	338 m	δ_{as}(CSO)
			388 m	381 m	δ_s(CSO)
403 w					ν_s(CdO)
	419 m	418 m[a,b]			ν_{as}(MnO)
459 m					δ_d(OClO) E
625 m	628 m	624 m[b]			δ_d(OClO) F_2
		662 vw[b]		612 sh	ν_s(CS)
679 vst	678 w	677 w[b]	663 vst	663 m	ν_s(CS)
714 st	714 m	717 m[b]	700 m	700 st	ν_{as}(CS)
910 w	904 w		900 vw	900 w	$\rho(CH_3)$
934 vst	941 sh				ν_s(ClO) A_1
		941 st[b]	925 vw	931 m	$\rho(CH_3)$
962 w	955 st	952 st[b]	954 w	955 st	$\rho(CH_3)$
1006 w		995 st[b]			$\rho(CH_3)$
1028 m	1011 vst	1012 st[b]			ν_s(SO)
1042 m		1039 sh[b]	1050 m	1050 vst	ν_s(SO)
1096 m	1100 sh	1098 vst[b]			ν_d(ClO) F_2
	1123 st	1126 vst[b]			ν_d(ClO) F_2
	1297 vw	1299 sh[b]		1303 m	δ_s(HCH)
	1318 m	1319 m[b]	1313 w		δ_s(HCH)
	1384 vw	1377 m[b]			δ_{as}(HCH)
1422 st	1416 m	1414 sh[b]		1404 st	δ_{as}(HCH)
	1437 m	1456 vst[b]	1425 m	1440 st	δ_{as}(HCH)
2816 sh		2857 vst[b]	2885 br	2825 br	ν_s(CH)
2867 sh		2870 sh[b]			ν_s(CH)
2922 vst	2917 m	2922 vst[b]	2913 vst	2910 st	ν_s(CH)
		2958 vst[b]			ν_{as}(CH)
	2995 sh		2999 m	2999 st	ν_{as}(CH)
3009 st	3000 m	3008 m[b]			ν_{as}(CH)

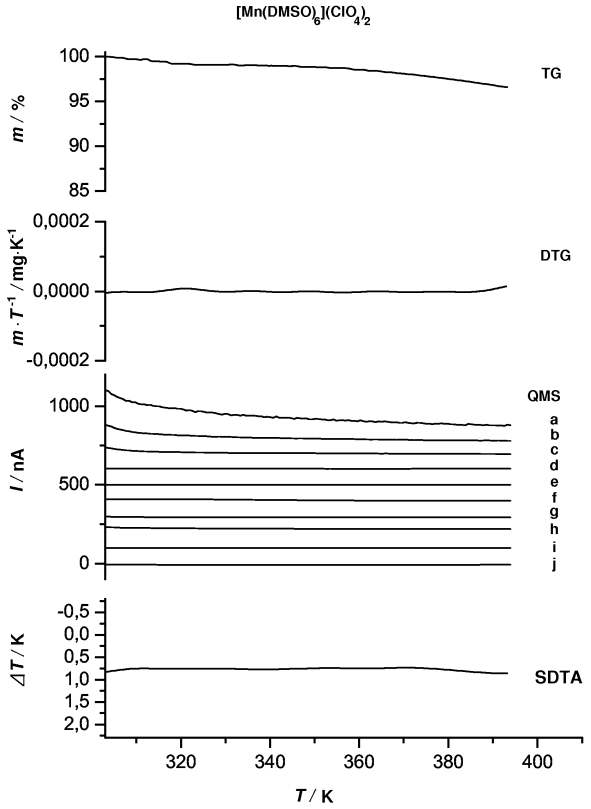

Fig. 2. TG, DTG, QMS and SDTA curves for HMnC at 303 – 393 K. (a, signal of $m/e = 18$; b, $m/e = 17$; c, $m/e = 16$; d, $m/e = 48$; e, $m/e = 14$; f, $m/e = 44$; g, $m/e = 13$; h, $m/e = 15$; i, $m/e = 32$; j, $m/e = 64$).

also registered. The temperature was measured by a Pt-Pt/Rh thermocouple with an accuracy of ± 0.5 K. Figure 2 presents a comparison of the TG, DTG, QMS and SDTA curves for HMnC within the temperature range of 300 – 380 K. For reasons of graphic clarity, only the masses of *m/e* = 13, 14, 15, 16, 17, 18, 32, 44, 48 and 64 – representing the fragments: CH, CH_2, CH_3, CH_4 or O, OH, H_2O, S or O_2, CO_2, SO and SO_2 [of $(CH_3)_2SO$ fragmentation] are shown. It can be seen from TG and DTG curves that during heating from RT up to 393 K the sample does not lose more than ca. 2% of its initial mass. This means that the title compound practically does not change its chemical composition in temperature range covering the detected phase transitions, even when the sample is not hermetically confined. Moreover, the absence of peaks both on QMS and on DTA curves, additionally confirms that the statement presented above is true.

To sum up, the FT-RS, FT-FIR and FT-MIR spectra, the thermal analysis (TG, DTA), mass spectroscopy (QMS) and chemical analysis have jointly certified the purity and proper composition of the examined compound. However, it should be stressed that the investigated compound is not very stable and starts losing $(CH_3)_2SO$ molecules, already at room temperature, of course when it is not hermetically confined.

Table 2. Thermodynamics parameters of the detected phase transitions (on heating).

	$[Mn(DMSO)_6](ClO_4)_2$		
	T_c	ΔH	ΔS
	K	$kJ\,mol^{-1}$	$J\,mol^{-1}\,K^{-1}$
T_m	487.65 ± 3.00	37.83 ± 1.30	184.48 ± 2.90
T_{C1}	$378.66 \pm 1{,}10$	3.43 ± 0.40	9.07 ± 1.06
T_{C2}	375.66 ± 2.25	4.44 ± 0.45	11.83 ± 1.21
T_{C3}	364.66 ± 3.00	27.11 ± 1.24	74.33 ± 2.86
T_{C4}	321.56 ± 2.53	16.60 ± 0.62	51.63 ± 1.82
T_{C5}	225.40 ± 0.09	0.88 ± 0.11	1.99 ± 0.25

2.3. Heat Flow Measurements

The DSC measurements of HMnC were made using two types of DSC apparatus: the first one was a Perkin-Elmer DSC-7 apparatus used in the temperature range of 173 – 520 K for samples hermetically confined in 30 μl aluminium containers. The weight of that sample was 10.90 mg (sample *a*). Details of the DSC experiment are the same as described in [9]. The second one was a Perkin-Elmer PYRIS 1 DSC apparatus on which three samples were investigated in the temperature range of 173 – 400 K. The weight of these samples was respectively: 16.16 mg (sample *b*), 6.32 mg (sample *c*) and 12.46 mg (sample *d*). The experimental details were the same as published in [10].

3. Results and Discussion

The temperature dependencies of the difference in thermal power supplied to the two calorimeters (the so-called thermal stream or heat flow), named DSC curves, were obtained for each of four HMnC samples at different scanning rates and at different initial and final sample heating and cooling conditions. Masses of the samples were chosen as to determine whether the observed phase transition depended on the sample weight, or not. We did not notice significant differences between the results for the samples *a*, *b*, *c* and *d*. All thermodynamic parameters of the phase transitions are put together in Table 2. The results of all DSC measurements are schematically presented altogether as a temperature dependence of the free enthalpy *G* (Gibbs free energy) and shown in Figure 3.

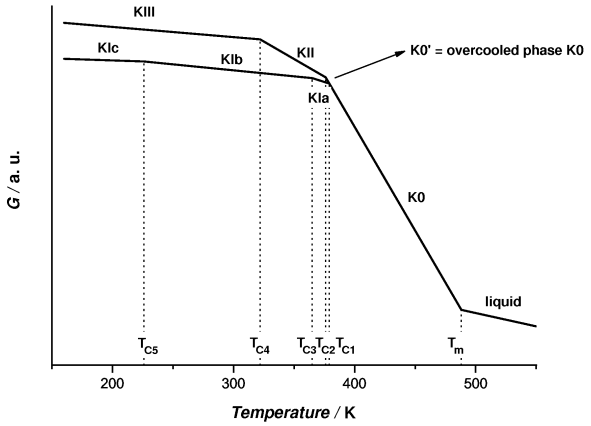

Fig. 3. Scheme of the temperature dependence of the free enthalpy G of HMnC.

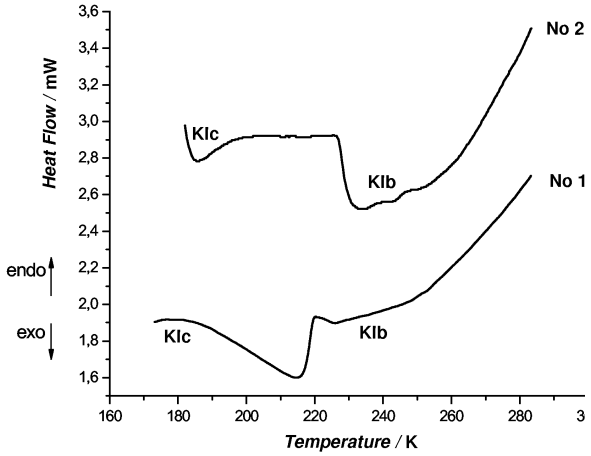

Fig. 4. DSC curves obtained during heating (curve No 1) and during cooling in the temperature range of 173 – 298 K (curve No 2) of HMnC with a scanning rate of 30 K/min.

All investigated samples, not yet subjected to any "thermal history", so-called "virgins", are in a crystalline phase described as a KIb phase. The measurements on sample *a* were started by cooling the sample from room temperature (RT) to 173 K, holding it at this temperature for l min, then heating it up to 393 K and then cooling it again down to 173 K. The DSC curves obtained on first cooling (curve No 1) and subsequent heating (curve No 2) of sample *a*, with a scanning rate of 30 K/min, are shown in Figure 4. As can be seen in Fig. 4, during cooling and heating the sample *a*, displays at ca. 225 K on both DSC curves a small exothermic and endothermic anomaly, respectively, which is connected with the reversible solid phase transition: the KIb phase ↔ the KIc phase (compare with diagram in Fig. 3). This anomaly was recorded also for the "virgin" samples *b* and *c*, which were cooled down to 153 K and then heated up to 393 K. For sample *d* the anomaly was not recorded, probably because of the low value of the sample weight and too high value of the scanning rate (40 K/min). This transition temperature was marked as $T_{C5} = 225$ K.

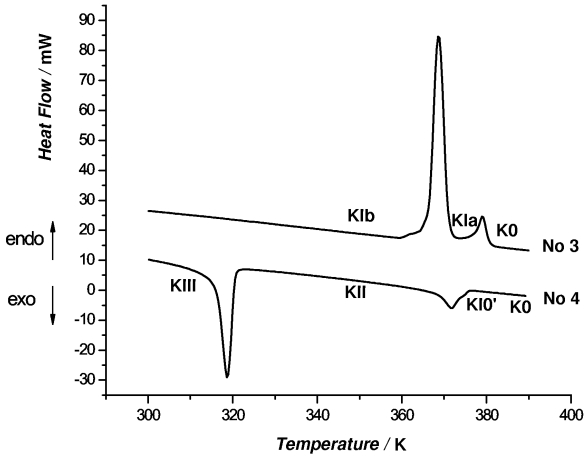

Fig. 5. DSC curves registered during heating from 293 to 393 K (curve No 3) and during cooling at 293 – 393 K (curve No 4) of HMnC with a scanning rate of 20 K/min.

While heating sample *b* from 273 K till 393 K, being initially in the KIb phase, it undergoes the phase transition at $T_{C3} = 365$ K into the KIa phase, which goes next at $T_{C1} = 379$ K into the K0 phase (compare with Fig. 3). Due to this transition, distinct anomalies on the DSC curves were recorded for all four samples *a*, *b*, *c* and *d*. For example, Fig. 5 shows these anomalies recorded at $T_{C3} = 365$ K and at $T_{C1} = 379$ K for sample *b* with a heating rate of 20 K/min (curve No 3). While cooling sample *b* in the K0 phase from 393 K till 273 K, a slight overcooling was observed. The overcooled K0 phase undergoes the metastable phase at $T_{C2} = 376$ K, described as the KII phase. Being further cooled down, the KII phase goes next at $T_{C4} = 322$ K into the KIII phase (compare with Fig. 3). The phase transitions at T_{C2} and at T_{C4} were recorded on the DSC curves as anomalies connected with exothermic processes for all four samples *a*, *b*, *c* and *d*. For example, these two anomalies were showed for sample *b* in Fig. 5 (curve No 4).

The phase transitions from the overcooled K0 phase to the KII phase (at T_{C2}) and from the KII phase to the KIII phase (at T_{C4}) are reversible. This is clearly visible in Fig. 6, showing for example DSC curves that

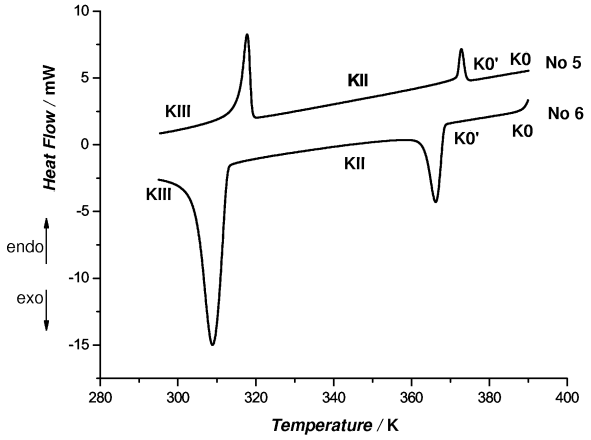

Fig. 6. DSC curves registered during heating from 293 to 393 K (curve No 5) and during cooling at 393 – 293 K (curve No 6) of HMnC with a scanning rate of 10 K/min.

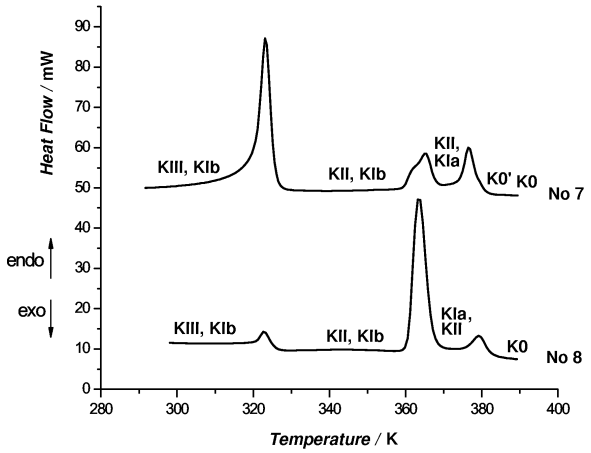

Fig. 7. Comparison of the DSC curves registered during heating from 298 to 393 K with a scanning rate of 30 K/min (curve No 7) and 40 K/min (curve No 8) in two different sets of measurement conditions.

were recorded during heating (curve No 5) and cooling (curve No 6) sample *a* in the temperature range of 293 – 393 K with a rate of 10 K/min. Both during heating and cooling, two distinct anomalies on the DSC curves occured that were due to both detected phase transitions: the overcooled K0 phase ↔ KII phase and the KII phase ↔ KIII phase.

In order to better clarify the metastable character of phases KII and KIII, in Fig. 7 we have compared the DSC curves registered at two different initial conditions of the measurements. On the DSC curve No 7 we can see one major anomaly at T_{C4}, connected with the transition from metastable phase KIII to metastable phase KII, and a doublet anomaly at T_{C3}, connected

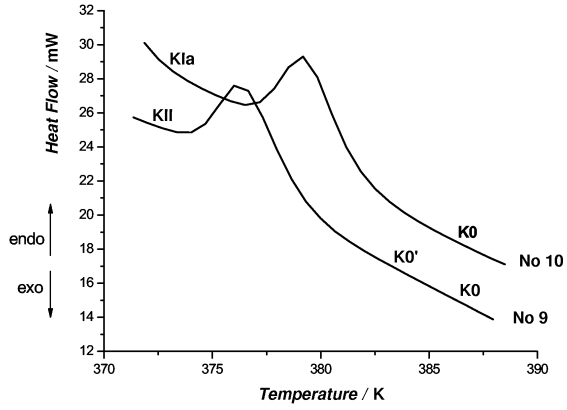

Fig. 8. Comparison of the DSC curves registered during heating from 370 to 393 K with a scanning rate of 40 K/min at two different conditions of measurements.

with the phase transition stable phase KIb → stable phase KIa and a single anomaly at T_{C2}, connected with the phase transition metastable phase KII → stable phase K0. On the DSC curve No 8 we can see one slight anomaly at T_{C4}, connected with the phase transition metastable phase KIII ↔ metastable phase KII, one major anomaly at T_{C3}, connected with the phase transition stable phase KIb → stable phase KIa and a slight one at T_{C1}, connected with the phase transition stable phase KIa → stable phase K0. Curve No 7 was obtained during heating the sample immediately after cooling it to 193 K, whereas curve No 8 was obtained during heating the sample and also cooling down to 193 K but only after holding it at this temperature for 5 min. Thus, in this second case, because of the slow spontaneous conversion of a large part of the metastable phase KIII, first probably into the stable phase KIc and next into the stable phase KIb, we can see on curve No 8 the small anomaly at T_{C4} and big one at T_{C3}, connected with the KIII → KII and KIb → KIa phase transitions, respectively. On curve No 7 quite an opposite phenomenon has occurred; one can observe a major anomaly at T_{C4} and a slight one at T_{C3}, because in this case only a small part of the metastable phase KIII had converted into the stable phases KIc and/or next KIb. Moreover, on curve No 7 one can see only the anomaly at T_{C2}, and one does not see the anomaly at T_{C1}, whereas on curve No 8 the situation is reversed. This has occurred due to the fact that in the second case the metastable phase KII was partially converted into the stable KIb phase and afterwards completely converted into the KIa phase.

In spite of very small differences between the phase transition temperatures and also of enthalpy changes,

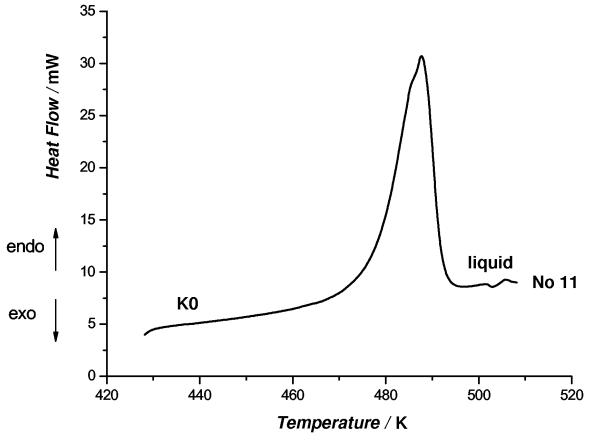

Fig. 9. DSC curve registered in the temperature range of 420 – 520 K during heating of HMnC with a scanning rate of 25 K/min.

the phase transitions undergoing at T_{C2} and at T_{C1} consist actually of two different phase transitions. Namely: Fig. 8 presents the comparison of the two curves obtained at heating same sample *c* with the same scanning rate of 40 K min^{-1} but after two different "thermal histories". On curve No 9 we can see the anomaly at T_{C2} connected with the KII → K0 phase transition, because the sample was earlier cooled fast (30 K min^{-1}) to the phase KII. On curve No 10 we can see an anomaly at T_{C1} connected with the KIa → K0 phase transition, because the sample was cooled slowly (10 K min^{-1}) exactly as in phase KIa.

Of course it is not possible to determine the nature of the observed phases only on the basis of DSC measurements. However, it was observed with a microscope that all the phases proceed in the solid state. Moreover, it was verified by X-ray powder diffraction measurements, which are now in elaboration in order to determine the crystal structure of all discovered phases of the title compound [11].

Additionally, it was concluded from the enthalpy change ΔS at the T_{C3} and T_{C4} phase transitions (see Table 2), that the phases KII and KIa are in high rotational disorder, so that they are called "orientationally dynamically disordered crystals" (ODIC). The phases KIc, KIb, and K0 are more or less the ordered ones (small ΔS values connected with the KIc → KIb and KIa → K0 phase transitions, registered at T_{C5} and T_{C1}, respectively). The KIII and KII phases form mutually an enantiotropic system but, in a relation to the KIa, KIb and KIc phases, they are metastable in the whole temperature range, and thus they form a monotropic system.

When heated up above T_{C1} the sample melts at $T_m = 488$ K. A subsequent DSC curve, showing the anomaly resulting from the melting process, can be seen in Fig. 9 (curve No 11).

4. Conclusions

1. The thermodynamic parameters for the following phase transitions of HMnC have been determined:

• reversible phase transition: stable KIc ↔ stable KIb at $T_{C5} = 225$ K;

• reversible phase transition: metastable KIII ↔ metastable KII at $T_{C4} = 322$ K;

• irreversible phase transition: stable KIb → stable KIa at $T_{C3} = 365$ K;

• reversible phase transition: metastable KII ↔ overcooled K0 at $T_{C2} = 376$ K;

• irreversible phase transition: KIa → K0 at $T_{C1} = 379$ K;

• melting of the crystals at $T_m = 488$ K.

2. It can be concluded from the enthalpy values of the transitions, that the phases KII and KIa are phases of high rotational disorder ["orientationally dynamically disordered crystals" (ODIC)]. Phases KIc, KIb, and K0 are more or less ordered. Contrary to HCdC and HCoC the enthalpy change connected with the melting of HMnC is evidently higher than their values for the order-disorder phase transitions at T_{C3} and T_{C4}.

Acknowledgements

Our thanks are due to Prof. Dr. S. Wróbel from the Faculty of Physics, Astronomy and Applied Computer Science of the Jagiellonian University for enabling us to perform the DSC measurements on the PYRIS 1 apparatus, and to Dr. hab. E. Mikuli from the Faculty of Chemistry of the Jagiellonian University for stimulating discussions. We are also grateful to J. Ściesiński, M. Sc. and Dr. hab. E. Ściesińska from the H. Niewodniczański Institute of the Nuclear Physics Polish Academy of Sciences in Kraków for the FT-FIR spectrum, to Dr. A. Wesełucha-Birczyńska from the Regional Laboratory of Physicochemical Analysis and Structural Research in Kraków for the FT-RS spectrum and Dr. M. Molenda from the Faculty of Chemistry of the Jagiellonian University for his help in the thermal analysis of the title compound.

[1] T. U. Lubeznowa and I. Ponomariew, Kristallografia **34**, 862 (1989).
[2] A. Migdał-Mikuli, E. Mikuli, E. Szostak, and J. Serwońska, Z. Naturforsch **58a**, 341 (2003).
[3] A. Migdał-Mikuli and E. Szostak, Thermochim. Acta **426**, 191 (2005).
[4] J. Selbin, W. E. Bull, and L. H. Holmes Jr., J. Inorg. Nucl. Chem. **16**, 219 (1961).
[5] F. A. Cotton, R. Francis, and W. D. Horrocks Jr., J. Phys. Chem. **64**, 1534 (1960).
[6] M. Sandström, I. Persson, and St. Ahrland, Acta Chem. Scand. **A 32**, 607 (1978).
[7] J. E. Connet, J. A. Creighton, J. H. S. Green, and W. Kynaston, Spectrochim. Acta **22**, 1859 (1966).
[8] Raman/IR Atlas. Verlag Chemie, Weinheim/Bergstraße, Germany 1974.
[9] E. Mikuli, A. Migdał-Mikuli, and J. Mayer, J. Thermal Anal. **54**, 93 (1998).
[10] A. Migdał-Mikuli, E. Mikuli, S. Wróbel, and Ł. Hetmańczyk, Z. Naturforsch. **54a**, 590 (1999).
[11] A. Migdał-Mikuli, E. Szostak, M. Bućko, and E. Mikuli, J. Solid St. Chem., in press.